



Accepted Article

Title: Unveiling the photoinduced electron-donating character of MoS2 in covalently linked hybrids featuring perylenediimide

Authors: Ioanna K. Sideri, Youngwoo Jang, Jose Garcés-Garcés, Ángela Sastre-Santos, Ruben Canton-Vitoria, Ryo Kitaura, Fernando Fernández-Lázaro, Francis D'Souza, and Nikos Tagmatarchis

This manuscript has been accepted after peer review and appears as an Accepted Article online prior to editing, proofing, and formal publication of the final Version of Record (VoR). This work is currently citable by using the Digital Object Identifier (DOI) given below. The VoR will be published online in Early View as soon as possible and may be different to this Accepted Article as a result of editing. Readers should obtain the VoR from the journal website shown below when it is published to ensure accuracy of information. The authors are responsible for the content of this Accepted Article.

To be cited as: Angew. Chem. Int. Ed. 10.1002/anie.202016249

Link to VoR: https://doi.org/10.1002/anie.202016249

WILEY-VCH

RESEARCH ARTICLE

Unveiling the photoinduced electron-donating character of MoS₂ in covalently linked hybrids featuring perylenediimide

Ioanna K. Sideri, [a] Youngwoo Jang, [b] Jose Garcés-Garcés, [c] Ángela Sastre-Santos, [c] Ruben Canton-Vitoria, [d] Ryo Kitaura, [d] Fernando Fernández-Lázaro, *[c] Francis D'Souza, *[b] and Nikos Tagmatarchis*[a]

- [a] I. K. Sideri, Prof. Dr. N. Tagmatarchis
 Theoretical and Physical Chemistry Institute
 National Hellenic Research Foundation
 48 Vassileos Constantinou Avenue, 11635 Athens (Greece)
 E-mail: tagmatar@eie.gr
- [b] Y. Jang, Prof. Dr. F. D'Souza Department of Chemistry University of North Texas 1155 Union Circle, 305070 Denton, TX 76203-5017 (USA) F-mail: Francis DSouza@unt edu
- [c] J. Garcés-Garcés, Prof. Dr. Á. Sastre-Santos, Prof. Dr. F. Femández-Lázaro Área de Química Orgánica, Instituto de Bioingeniería Universidad Miguel Hernández 03202, Elche (Spain)
- [d] Dr. R. Canton-Vitoria, Prof. Dr. R. Kitaura Department of Chemistry Nagoya University 464-8602, Nagoya (Japan)

Supporting information for this article is given via a link at the end of the document.

Abstract: The covalent functionalization of MoS₂ with a perylenediimide (PDI) is reported and the study is accompanied by detailed characterization of the newly prepared MoS₂-PDI hybrid material. Covalently functionalized MoS₂ interfacing organic photoactive species have shown electron and/or energy accepting, energy reflecting or bi-directional electron accepting features. Herein, a rationally designed PDI, unsubstituted at the perylene core to act as electron acceptor, forces MoS₂ to fully demonstrate for the first time its electron donor capabilities. The photophysical response of MoS₂-PDI is visualized in an energy-level diagram, while femtosecond transient absorption studies disclose the formation of MoS₂+PDI-charge separated state. The tunable electronic properties of MoS₂, as a result of covalently linking photoactive organic species with precise characteristics, unlock their potentiality and enable their application in light-harvesting and optoelectronic devices.

Introduction

Targeting molybdenum disulfide (MoS₂) implementation in practical electronic devices and energy harvesting and storage area, tailoring of its properties is of paramount importance. Towards this goal, chemical functionalization of MoS₂ constitutes an emerging area of interest that achieves the manipulation of MoS₂ existing properties and the acquisition of novel qualities. Two main pillars have been recently established for the covalent functionalization of 2H-MoS₂, which are the S-defects' healing with sulfur compounds (thiol, I² dithiolane I³ and dithiolene I⁴ moieties) and the organic/organometallic reaction pathways, involving S_N2 substitution I⁵ and metal coordination. I⁶

Perylenediimides (PDIs) are extremely versatile organic molecules that are characterized by light-absorbing properties, near-unity fluorescence quantum yields and exciton mobility. [7]

Apart from these qualities, their spatial distribution is interesting, since they are prone to aggregated architectures [8] and hydrogenbond directed self-assemblies, [9] that enable also charge-separation and charge-carrier properties. [10] Interestingly, these unique characteristics vary, depending on perylenes' type and location of substituents. [11] Imide-substituted PDIs without substituents on the perylene core are n-type semiconductors and are widely used as electron acceptors in organic photovoltaics. Conversely, bay-substituted perylenes demonstrate from π -acceptor to strong π -donor character based on the nature of their substituents. Therefore, custom-synthesis enables PDIs to excel in plethora of cutting-edge technological applications, such as organic transistors, [12] photovoltaics [13] and photonics. [14]

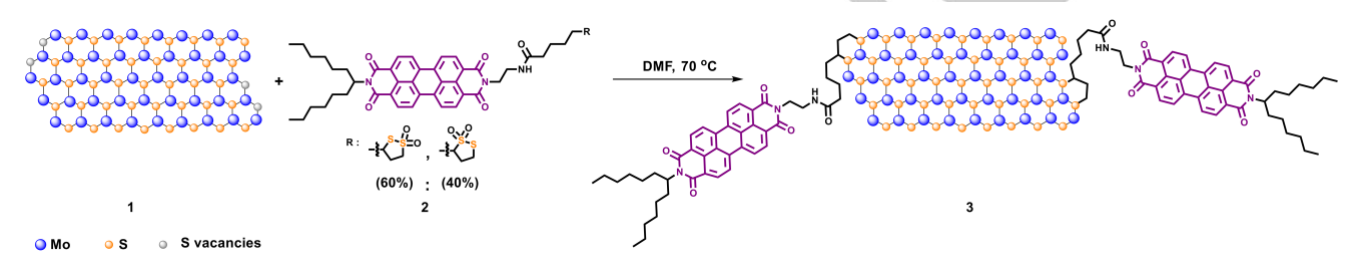
Based on our previously reported series of covalently functionalized MoS2 with organic photoactive species, different photophysical response has been registered for the various MoS₂ based materials. Namely, the MoS₂ entity may act as electron and/or energy acceptor,[15] energy reflector[16] or bi-directional electron acceptor.[17] based on the nature of its photoactive counterpart. Furthermore, there is a scarce literature report on a MoS₂/PDI interfacial dipole heterosystem, formed by noncovalent interactions between the two entities lacking significant insight into MoS₂ charge transfer properties.^[18] Therefore, it is timely and imperative to go beyond the existing knowledge of covalent hybrids of MoS₂ as electron acceptors. Herein, aiming in unveiling MoS2 electron donor capabilities, we envisioned a novel MoS₂-perylenediimide conjugate, where its photoinduced processes are examined. Bringing our plan into existence, a core unsubstituted PDI derivative, with proven electron-accepting character, carrying a thiosulfonate moiety, was rationally designed, synthesized and covalently attached to MoS2 Sdefected edges. Next, we employed a series of techniques for characterizing the MoS₂-PDI hybrid material, followed by redox, spectroelectrochemical and photophysical assessment.

Femtosecond transient absorption spectroscopy (fs-TA) revealed the formation of the MoS₂⁻⁺-PDI⁻⁻ charge separated state by reductive electron transfer to ¹PDI* from MoS₂. Our results expand the portfolio of species with which MoS₂ can interface towards the realization of functional nanohybrids for managing charge-transfer phenomena.

Results and Discussion

Exfoliated MoS₂ **1** was prepared by liquid chemical exfoliation,^[19] while the PDI derivative **2**, featuring a thiosulfonate ring, was synthesized via a condensation reaction of the amino-substituted PDI with lipoic acid and was fully characterized by NMR, MALDI-

TOF-MS and IR spectroscopy (**Figures S1-S6**). The thiosulfonate structure of the ring is confirmed by IR spectroscopy, since the two characteristic bands at 1340 cm⁻¹ and 1127 cm⁻¹ attributed to the sulfone moiety are present (**Figure S6**). Compound **2** is actually a 60:40 mixture of the two possible isomers formed by oxidation of each sulfur atom (see Supporting Information for details). Next, reaction between the two species in *N,N*-dimethylformamide (DMF) furnished MoS₂-PDI hybrid material **3** (**Scheme 1**), in which S-vacancies at the periphery of MoS₂ are occupied by the S atoms of the ring as part of PDI derivative. [3,15-17] After completion of the reaction, total removal of excess **2**, from the powder residue obtained, was secured by filtration over PTFE membrane filter (0.2 μm pore size) and extensive washing with dichloromethane, as evidenced upon blank absorbance of the filtrate (**Figure S7**).



Scheme 1. Illustration of the chemical reaction of exfoliated MoS₂ 1 with PDI derivative 2, furnishing MoS₂-PDI hybrid material 3.

Raman spectroscopy assays (λ_{exc} 633 nm) on 1 and 3 revealed all characteristic bands of MoS2. The fingerprint of MoS2 includes three modes in the range of 300-500 cm⁻¹, which are E¹_{2g} at 375 cm⁻¹, A_{1g} at 405 cm⁻¹ and 2LA(M) at 450 cm⁻¹. While the former two modes (E12g and A1g) are associated with in- and outof-plane vibrations, the latter 2LA(M) is defect-induced and specifically, S-vacancy-related. [20] In Figure 1a, the Raman spectrum of MoS2-PDI hybrid material 3 is compared with that of exfoliated MoS2, where a clear decrease in the 2LA(M) mode intensity is observed after the functionalization reaction. Please note that while MoS₂ nanosheets with different size and thickness exist, every different MoS2 flake is functionalized in an uncontrollable fashion depending also on defect availability and accessibility in this particular manifold. Therefore, in order to have a generic image of the 2LA(M) mode intensity decrease upon functionalization, we visually represent in a form of 2D mapping assays, the intensity ratio $I_{A1g}\,/I_{2LA(M)}$ variation in a 30 μm x 30 μm area for both materials (Figures 1c and 1d). The fluctuation of the intensity ratio $I_{A1g} \ / I_{2LA(M)}$ is averaged at 0.99 for exfoliated MoS $_2$ (Figure 1c) and 1.34 for MoS₂-PDI hybrid material 3 (Figure 1d). This increase by around 35% upon functionalization, is attributed to the defect healing of MoS₂ layer due to the incorporation of the sulfur-containing chain featured in 2. In addition, information regarding the conductivity characteristics of the material is obtained, since the metallic polytype-related J_1 , J_2 and J_3 bands at 150, 225 and 325 cm⁻¹,[21] respectively, are absent in both Raman spectra of 1 and 3. Therefore, the semiconducting characteristics of the 2H-MoS2 polytype obtained with the exfoliation conditions are retained in the MoS₂-PDI hybrid material 3. Complementary, Raman spectrum of PDI derivative 2, under on-resonance conditions (λ_{exc} 514 nm), is characterized by eight well-resolved bands at 1292, 1376, 1595, 2589, 2668, 2750, 2868 and 2941 cm⁻¹, assigned to in-plane C-C stretch and in-plane C-C-H bend vibrations (Figure 1b).[22] Accordingly, these bands are present in the Raman spectrum (λ_{exc} 514 nm) of **3**, along with those of the MoS₂ fingerprint at 300-500 cm⁻¹, confirming the successful chemical modification.

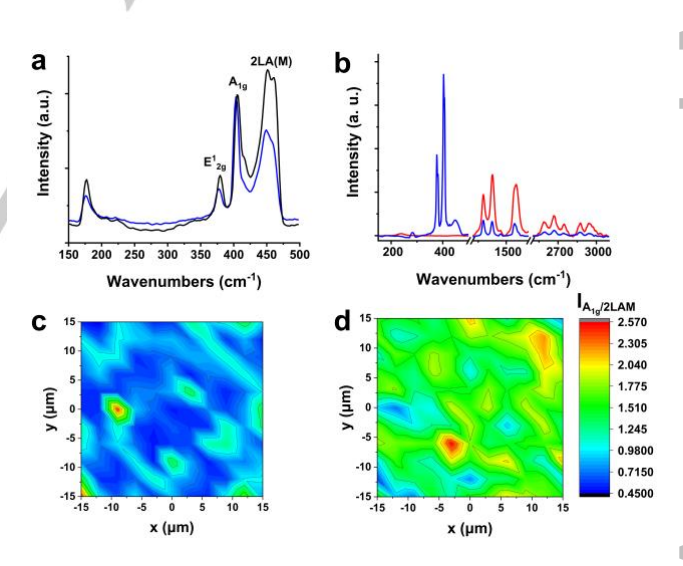


Figure 1. Raman spectra of a) exfoliated MoS $_2$ 1 (black) and MoS $_2$ -PDI hybrid material 3 (blue) upon excitation at 633 nm (spectra normalized at the A $_{1g}$ mode), and b) PDI derivative 2 (red) and MoS $_2$ -PDI hybrid material 3 (blue), upon excitation at 514 nm. Raman mapping, upon excitation at 633 nm, of the I $_{A1g}$ /I $_{2LA(M)}$ intensity ratio of a 30 µm x 30 µm area for c) exfoliated MoS $_2$ 1, and d) MoS $_2$ -PDI hybrid material 3.

ATR-IR spectroscopy studies on **3** further validated the above syllogism, since characteristic IR bands of PDI derivative **2** (**Figure S4**) are distinct on the ATR-IR spectrum of the hybrid material **3** (**Figure 2a**). Namely, the bands at 2800-2900 cm⁻¹ are assigned to the C-H stretching vibrations of the aliphatic chains of

PDI, the bands at 1690 cm⁻¹ and 1655 cm⁻¹ are attributed to the symmetric and asymmetric carbonyl stretch modes of the imide groups, the 1595 cm⁻¹ band is attributed to the conjugated C-C stretch modes of the aromatic system and the band at 746 cm⁻¹ is due to the C-S stretching vibration of the dithiolane moiety. Considering the strong evidence of the PDI presence in 3, along with the S-vacancies-related decreased 2LA(M) mode in the functionalized material and the respective work-up to remove any physisorbed species, we deduce that the PDI moieties are covalently attached to MoS₂ lattice.

Quantitative information for the degree of functionalization for 3 is obtained by thermogravimetric analysis (TGA). In Figure 2b, the TGA graphs under N₂ of the exfoliated MoS₂ 1, the PDI ligand 2 and the MoS₂-PDI hybrid material 3 are compared. Whereas exfoliated MoS₂ 1 is rather thermally stable, losing only 1.4% of weight up to 500 °C, due to lattice decomposition initiated by the S-defected areas, the organic addend 2 decomposes by 60% in the same temperature range. At the end of the analysis, 2 leaves behind a 20% residue due to the perylene aromatic core. On the other hand, hybrid material 3 exhibits a 4.9% mass loss up to 500 °C owing to the grafted perylene chains on the MoS2 periphery. Considering this mass loss and the molar masses of MoS₂ unit and PDI, the degree of functionalization is estimated as 1 PDI moiety per every 97 MoS₂ units, which is a relatively high loading considering the available S-vacancies located at the edges of the MoS₂ nanosheet.

Regarding the morphology of MoS₂-PDI hybrid material **3**, AFM analysis shows an average height of 2-3 nm, corresponding to an average of \sim 4 layers. Nevertheless, single layered MoS₂ was also found (**Figures 2c-d**) and the average length is 80x80 nm² with amorphous shapes. The absence of perylene-perylene agglomerations within hybrid material **3**, evidenced by the uniform height observation, is highlighted by a 3D-AFM image (**Figure S8**). In addition, MoS₂ layers do not show holes or presence of impurities, making an ideal system for further optoelectronic studies. Analyzing the height profile of a MoS₂ single layer in **3**, a reduction in height from the edge to the center of the layer is apparent, i.e. from 0.9 to 0.6 nm, suggesting that the chemical incorporation of PDI exclusively takes place at the edges of MoS₂.

High-resolution TEM imaging was further employed to understand the morphology of the hybrid material **3** at higher magnification. Although we focus on a single layer suspended on a TEM grid, the chemically modified MoS₂ layer is rough, producing valleys (**Figure 2e**). However, atoms can be easily distinguishable in several regions of the picture, without observing defects on the lattice. The absence of black areas on the imaged sample ensures lack of PDI and/or other organic species physisorbed onto the basal plane of MoS₂. In addition, we want to remark that the high perimeter-to-area ratio, observed by TEM and AFM, is in line with the relatively high level of functionalization estimated by TGA. Finally, EDX reveals the presence of appreciable amount of C as well as O due to PDI, on top of Mo and S in **3** (**Figure 2f**).

Electronic absorption spectroscopy constitutes an effective means of characterizing chemical states in PDI chemistry. PDI's vibronic progression, that is the typical electronic S_0 - S_1 transition, results in three well-defined bands in its absorption spectra at 456, 489 and 525 nm.^[23, 24] These characteristic bands are attributed to the 0-2, 0-1 and 0-0 transitions, respectively (**Figure 3a**). Conversely, the exfoliated 2H-MoS $_2$ absorption spectrum is dominated by four broad bands centered at 690, 630, 470, and

400 nm, which reveal the prominent semiconducting character of the material. The former two bands at 690 and 630 nm are the A and B excitonic transitions, while the direct transitions from the valence to the conduction band are represented by the C and D bands at 470 and 400 nm, respectively [25] (Figure 3b). The UV-Vis spectrum of hybrid material 3, highly resembles that of exfoliated MoS2 since the aforementioned A, B, C and D bands exist, corroborating the maintenance of the MoS₂ 2H phase upon covalent modification (Figure 3b). On the contrary, the signature bands of PDI are overshadowed by the C and D bands of MoS2 and therefore are revealed only upon subtraction of the absorbance spectrum of 1. At the inset of Figure 3b, the UV-Vis spectrum of 3 after subtraction of exfoliated MoS₂ 1 absorbance, is comparison with the same optical concentration (e.g. same intensity of 525 nm absorbance band) spectrum of 2. The absence of significant alterations in the UV-Vis spectrum of MoS2-PDI 3, as compared to that of 1 and 2, manifests that negligible, if any at all, electronic interactions between the two species within the hybrid material at the ground state, exist.

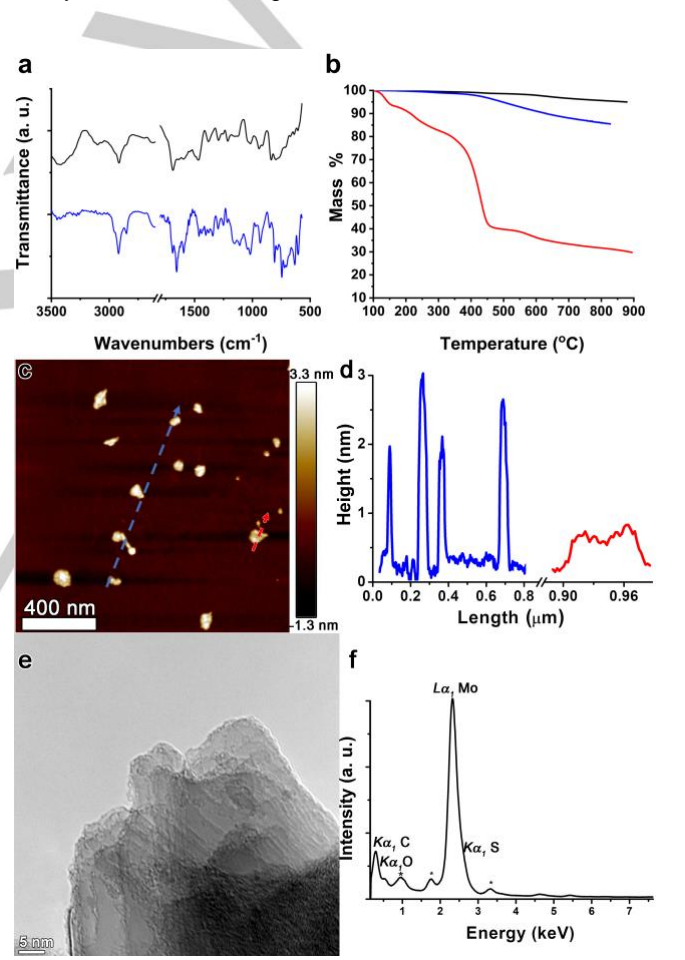


Figure 2. (a) ATR-IR spectra of exfoliated MoS_2 1 (black) and hybrid material 3 (blue). (b) TGA graphs for exfoliated MoS_2 1 (black), hybrid material 3 (blue) and PDI derivative 2 (red), obtained under N_2 atmosphere. (c) AFM image of hybrid material 3, and (d) the corresponding line height profile. (e) HR-TEM and (f) EDX of hybrid material 3. Impurity denoted with * is due to Si.

The emission spectra of 2 and 3 upon excitation at 480 nm, for samples possessing same optical concentration, are shown in Figure 3c. The fluorescent profile of both materials mirrors the

absorbance profile of **2**, while considerable fluorescence quenching of PDI's emission at 535 nm is observed for MoS₂-PDI hybrid material **3** (**Figure 3c**). Furthermore, fluorescence lifetime assays upon excitation at 561 nm reveal a monoexponential decay profile of 4.58 ns for free PDI derivative **2** (red trace in **Figure 3d**), while for the MoS₂-PDI hybrid material **3**, the decay profile was within the time resolution of our instrument setup (< 200 ps), and appeared identical to the lamp profile (blue trace in **Figure 3d**). Collectively, the data acquired from both steady-state and time-resolved fluorescence emission spectroscopic assays validate the presence of a new deactivation pathway involving MoS₂ at the excited state.

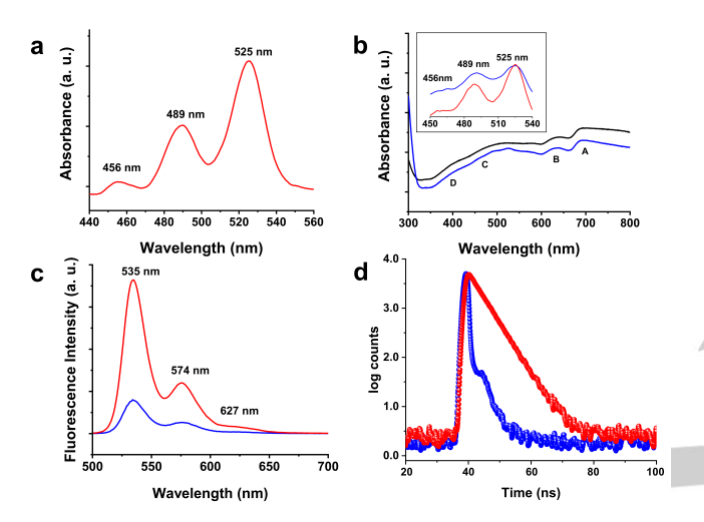


Figure 3. UV-Vis spectra of a) PDI derivative 2, b) exfoliated MoS_2 1 (black) and hybrid material 3 (blue). Inset: UV-Vis spectrum of 3 (blue) after subtraction of exfoliated MoS_2 1 absorbance in comparison with same optical concentration spectrum of 2 (red). c) Emission spectra of samples with same optical concentration of 2 (red) and 3 (blue), obtained upon excitation at 480 nm. d) Emission decay profiles of 2 (red) and 3 (blue), monitored at 574 nm, upon excitation at 561 nm. Time profile of 3 resembles that of lamp profile due to lifetime shorter than the time resolution of the instrument setup. All spectra were recorded in DMF

Next, the redox properties of MoS₂-PDI hybrid material **3** were assessed in benzonitrile vs Fc/Fc⁺ with the aid of cyclic voltammetry. The corresponding voltammogram is compared with those acquired from PDI derivative **2** and exfoliated MoS₂ **1** (**Figure S9**). Briefly, **2** exhibits two reversible reductions at -1.28 and -1.67 V, since perylenediimide is characterized by high electron affinity, allowing its facile reduction while rather hindering its oxidization.^[26] For exfoliated MoS₂, two irreversible reductions at -1.25 and -1.60 V and an irreversible oxidation at -0.18 V are registered.^[25] Regarding **3**, overlapped reduction signals that appear broadened, sum up to two irreversible reductions at -1.29 and -1.53 V. This small negative shift, by 10 mV, in the first reduction potential of PDI, calls for its harder reduction in hybrid material **3**.

From the earlier discussed optical and electrochemical results, an energy level diagram is established (**Figure 4**) to weigh in the possibility of reductive electron transfer to ¹PDI* from MoS₂ to yield MoS₂**-PDI*. The electrochemical gap in **3**, *viz.*, potential difference between the first oxidation of MoS₂ and first reduction of PDI ca. 1.11 eV, is smaller than the pumping energy of ¹PDI*, (i.e. 2.34 eV, calculated from the midpoint energy of absorption and fluorescence bands in **2**). Upon excitation, MoS₂-¹PDI*

formed, could undergo either intersystem crossing to populate the ³PDI* or be involved in electron or energy transfer events. From the thermodynamic point of view, reductive electron transfer to yield MoS2'+-PDI'- is plausible. Interestingly, the energy level of ³PDI*, i.e. 1.07 eV^[27] is slightly lower by that of MoS₂'+-PDI'-, ca. 1.11 eV. Therefore, under such circumstances, MoS2*+-PDI*could directly undergo back electron transfer to the ground state, or populate the ³PDI*. Considering that at the pumping energy of 2.34 eV, direct band gap excitation of MoS₂ at ca. 1.83 eV is also possible (please note that the direct band gap of MoS2 cannot be observed by electronic absorption and/or fluorescence spectroscopy)[15b,17,25]. This is particularly true considering the broad absorption of MoS₂, covering the 350-800 nm range, providing slender chances of selective excitation of PDI in the hybrid material 3. Fortunately, as shown in Figure 4, both ¹PDI* and ¹MoS₂* are capable of promoting electron transfer to yield the charge-separated state MoS2*+-PDI*-.

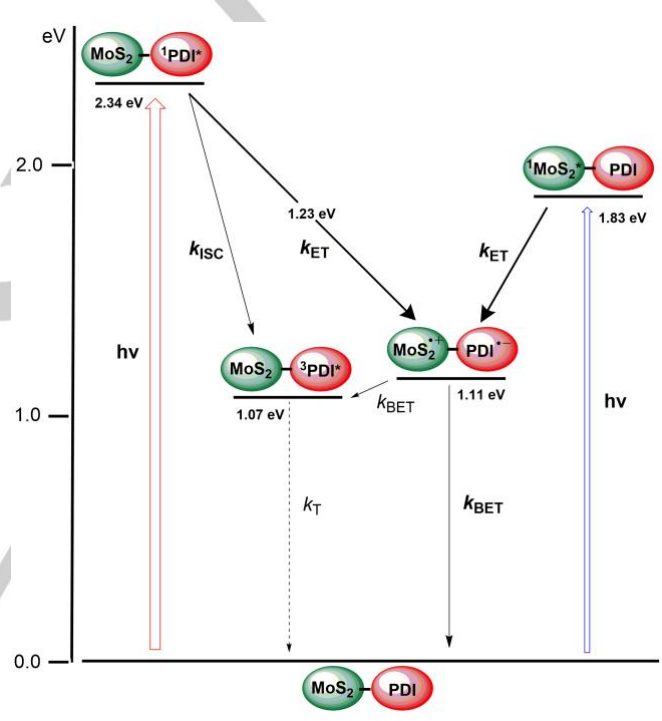


Figure 4. Energy level diagram depicting reductive electron transfer of ¹PDI* and oxidative electron transfer from ¹MoS₂* in the MoS₂-PDI hybrid material **3.** (thick arrows – most likely process; dotted arrow – less likely process, ET=electron transfer, BET=back electron transfer, T=triplet emission, ISC=intersystem crossing).

In order to characterize the anticipated electron transfer product, MoS2**-PDI*-, formed upon photoexcitation during transient absorption spectral studies, spectroelectrochemical studies were performed. The differential absorption spectrum of PDI*- obtained upon one-electron reduction of PDI 2 is shown in Figure 5c. Negative absorption bands at 460, 490 and 526 nm due to diminished concentration of neutral PDI, and new positive peaks at 680, 703, 711 and 767 nm corresponding to newly formed PDI*- are observed. Similar spectroelectrochemical studies, performed upon oxidation of exfoliated MoS2 1, revealed broad absorption covering the 300-800 nm region with a peak at ~440 nm as shown at the differential absorption spectrum in Figure 5f.

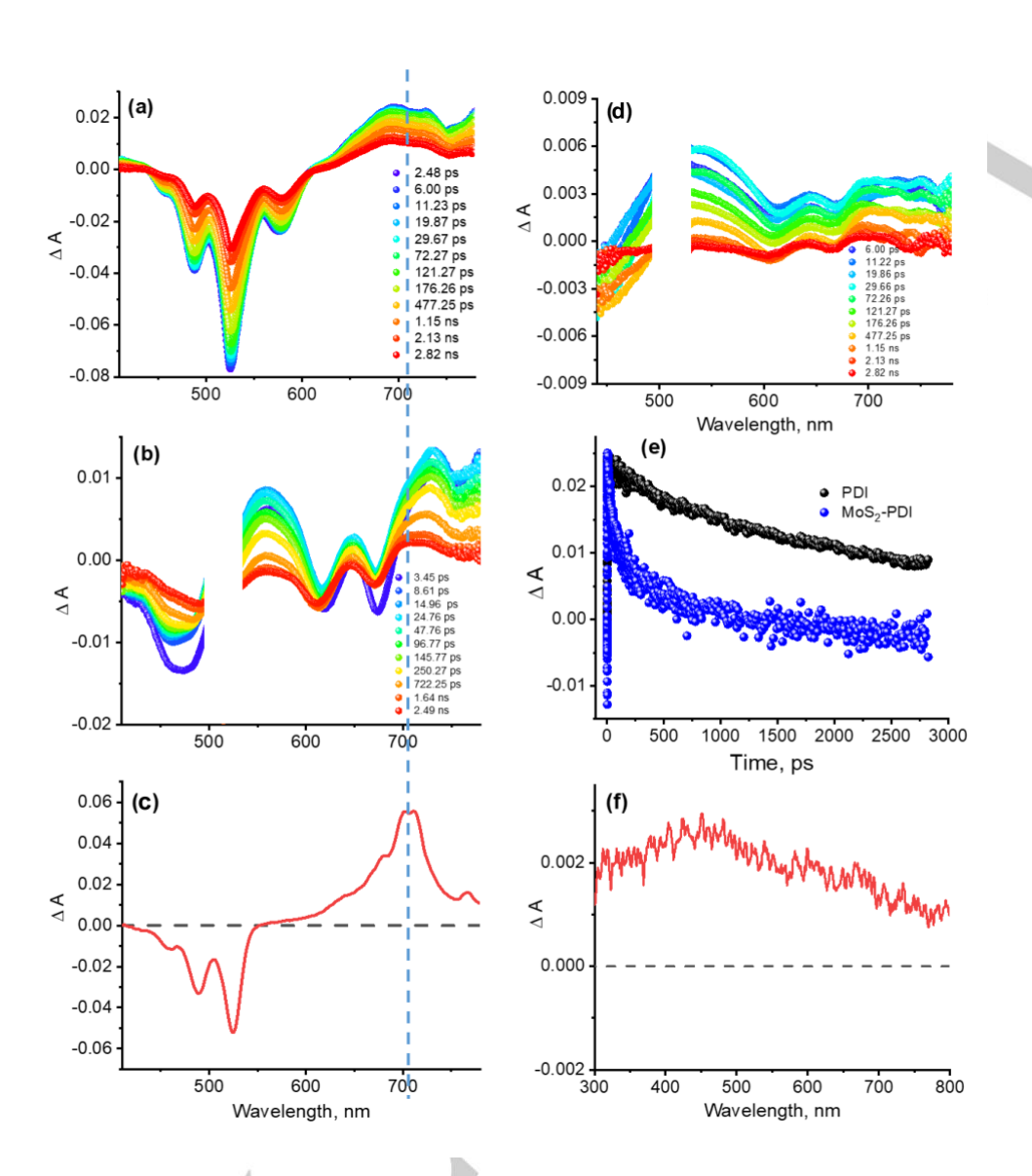


Figure 5. Femtosecond transient absorption spectra at the indicated delay times of (a) PDI derivative 2, (b) MoS₂-PDI hybrid material 3, and (d) exfoliated MoS₂ 1, upon excitation at 514 nm in DMF. (c) Differential absorption spectrum of one-electron reduced PDI⁻ in DMF. (e) Decay profile of the 784 nm peak corresponding to ¹PDI* of 2 (black) and 3 (blue). (f) Differential absorption spectrum for oxidized MoS₂⁻⁺ in DMF. The break in the 500-520 nm range is due to elimination of scattered light from excitation pulses.

Femtosecond transient absorption spectra (fs-TA) of PDI derivative **2**, at the indicated delay times, are presented in **Figure 5a**. The instantaneously formed ¹PDI* revealed excited state absorption bands at 694, 729 and 784 nm, accompanied by negative bands at 456, 488, 526 and 578 nm. Regarding the negative bands, the first two bands have contributions from ground state bleaching (GSB), while the last two bands have contributions from both GSB and stimulated emission. Decay and recovery of the positive and negative peaks is slow, consistent with the long lifetime of ¹PDI* (ca. 4.2 ns, also see decay profile of the 784 nm peak in **Figure 3d** (red trace)).

As shown in **Figure 5**, the spectral features of $^1PDI^*$, $^1MoS_2^*$ and PDI^- in the 625-750 nm range are close, and also due to lack of excitation wavelength selectivity, assigning of the transient peaks to a given species was rather challenging. However, careful

examination of spectral results is supportive of occurrence of charge separation in MoS₂-PDI hybrid material 3. As shown with the dashed line in Figures 5a and c, the main peak due to ¹PDI* centered at 694 nm is found to be slightly away from the PDI*peak at 711 nm. Due to lack of 100% excitation wavelength selectivity, the fs-TA spectra of MoS₂-PDI 3, shown in Figure 5b, revealed peaks corresponding to ¹PDI* along with additional peaks corresponding to ¹MoS₂*. Positive bands centered at 560, 648 and 717 nm, and negative peaks at 473, 618 and 675 nm are observed; that is, concurrent formation of ¹PDI* and ¹MoS₂* (induced absorption of B and A excitons having contributions in the 618, 675 and 710 nm peaks and negative peaks having contributions of GSB; $^{[15b,25]}$ see Figure 5d for fs-TA of MoS $_2$ excited at 514 nm) is witnessed. The decay/recovery of the singlet excited state peaks is associated with the slow development of a broad absorption band in the 710-715 nm range (different from

those of ¹PDI* and ¹MoS₂*), where peaks of PDI⁻ are expected, supporting occurrence of the anticipated charge separation. Additionally, the decay of the 784 nm peak, where contribution from ¹MoS₂* is minimal, is rapid, as shown in **Figure 5e** (blue trace), indicating involvement of ¹PDI* in the photoinduced reductive electron transfer process.

The. energy level diagram in **Figure 4** predicts population of ³PDI* during the process of charge recombination. Efforts were also made to spectrally characterize ³PDI* using nanosecond transient absorption (ns-TA) spectroscopy. Direct excitation of PDI gave no measurable signal, hence, ³PDI* was populated via energy transfer using anthracene, ^[28] as shown in **Figure S10**. Main peaks of ³PDI* spanned the 550-670 nm range. It is likely that the signature peaks of ³PDI, developed at a later time, are buried within the strong spectral features.

Having secured proof of occurrence of electron transfer in 3 to yield MoS2*+-PDI*-, next, we moved forward to secure time constant of this event. Transient data were subjected to Glotaran target analysis^[29] and species associated spectra (SAS) were generated, following the scheme shown in Figure 4. For satisfactory data fit, at least three SAS were needed, as shown in Figure 6a. The first SAS with a time constant of 1.69 ps (see Figure 6b for population-time plots) had contributions of the singlet excited states of the entities. The second component, with a time constant of 2.36 ns, had a characteristic peak of PDI* in the near-IR region and was attributed to the MoS2'+-PDI'- electron transfer product. The third component, with a time constant of 5.37 ns, had excitonic features of unmodified MoS₂ of similar time constant, [15b,17,25] and thus was attributed to free MoS2. The average time constant of 2.36 ns for the electron transfer product is reasonable considering the relatively long spacer between MoS₂ and PDI in the hybrid material 3.

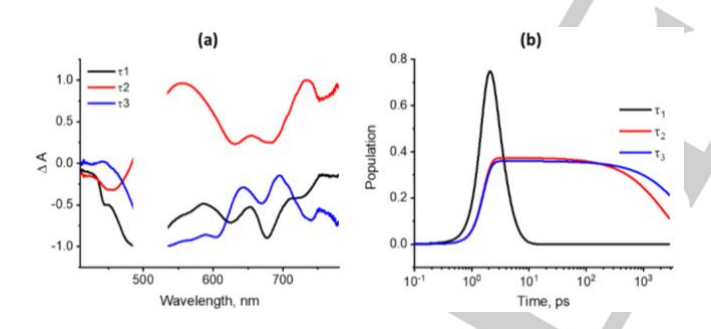


Figure 6. (a) Decay associated spectra and (b) population kinetics of MoS₂-PDI hybrid material **3** from Glotaran analysis of transient data shown in **Figure 5b**.The break in the 500-520 nm range is due to elimination of scattered light from excitation pulses.

Conclusion

In conclusion, an electron acceptor PDI derivative was covalently incorporated to semiconducting MoS_2 successfully, and a series of complementary characterization techniques were employed to outline the hybrid material's profile. The MoS_2 -PDI hybrid material 3 was custom-designed in order to complete the puzzle of MoS_2 possible photophysical charge-transfer events occurring in MoS_2 interfacing photoactive organic species. Steady-state and time-resolved photophysical assays together with redox and spectroelectrochemical studies acknowledge the formation of MoS_2^{*+} -PDI $^{*-}$ charge-separated state. Overall, the tunable

electronic properties of MoS₂, as a result of covalently linking photoactive organic species with precise characteristics, unlock their potentiality and enable their application in light-harvesting and optoelectronic devices.

Acknowledgements

Partial support of this work by the project "Advanced Materials and Devices" (MIS 5002409), which is implemented under the "Action for the Strategic Development on the Research and Technological Sector" funded by the Operational Program "Competitiveness, Entrepreneurship and Innovation" (NSRF 2014-2020) and co-financed by Greece and the European Union (European Regional Development Fund) is acknowledged. This material is also based upon work supported by the National Science Foundation under grant numbers 1401188 and 2000988 to FD and by European Regional Development Fund "A way to make Europe" and the Spanish Ministerio de Ciencia e Innovación/Agencia Estatal de Investigación through projects PID2019-109200GB-I00 and CTQ2017-87102-R (MCI/AEI/FEDER, UE). This project was also supported by Japan Society for the Promotion of Science (JSPS) postdoctoral fellowship grant agreement No P19368. We thank Prof. J. Ortiz for the acquisition of DEPT and HSQC spectra.

Keywords: perylenediimide • MoS₂ • covalent functionalization • charge-transfer • transient absorption spectroscopy

- [1] a) C. R. Ryder, J. D. Wood, S. A. Wells, M. C. Hersam, ACS Nano 2016, 10, 3900–3917; b) A. Stergiou, N. Tagmatarchis, Chem. Eur. J. 2018, 24, 18346
- a) S. S. Chou, M. De, J. Kim, S. Byun, C. Dykstra, J. Yu, J. Huang, V. P. Dravid, J. Am. Chem. Soc. 2013, 135, 4584-4587; b) Q. Ding, K. J. Czech, Y. Zhao, J. Zhai, R. J. Hamers, J. C. Wright, S. Jin, ACS Appl. Mater. Interfaces 2017, 9, 12734-12742.
- [3] a) R. Canton-Vitoria, Y. Sayed-Ahmad-Baraza, M. Pelaez-Fernandez, R. Arenal, C. Bittencourt, C. P. Ewels, N. Tagmatarchis, NPJ. 2D Mater. Appl. 2017, 1, 13; b) R. Canton-Vitoria, C. Stangel, N. Tagmatarchis, ACS Appl. Mater. Interfaces 2018, 10, 23476-23480.
- [4] I. K. Sideri, R. Arenal, N. Tagmatarchis, ACS Mater. Lett. 2020, 2, 832-937
- [5] a) S. Karunakaran, S. Pandit, B. Basu, M. De, J. Am. Chem. Soc. 2018, 140, 12634-12644; b) X. S. Chu, A. Yousaf, D. O. Li, A. A. Tang, A. Debnath, D. Ma, A. A. Green, E. J. G. Santos, Q. H. Wang, Chem. Mater. 2018, 30, 2112- 2128; c) M. Vera-Hidalgo, E. Giovanelli, C. Navío, E. M. Perez, J. Am. Chem. Soc. 2019, 141, 3767-3771.
- [6] C. Backes, N. C. Berner, Xi. Chen, P. Lafargue, P. LaPlace, M. Freeley, G. S. Duesberg, J. N. Coleman, A. R. McDonald, *Angew. Chem., Int. Ed.* 2015, 54, 2638-2642.
- [7] a) F. Würthner, C. R. Saha-Möller, B. Fimmel, S. Ogi, P. Leowanawat, D. Schmidt, Chem. Rev. 2016, 116, 962-1052.
- [8] A. Oleson, T. Zhu, I. S. Dunn, D. Bialas, Y. Bai, W. Zhang, M. Dai, D. R. Reichman, R. Tempelaar, L. Huang, F. C. Spano, J. Phys. Chem. C 2019, 123, 20567-20578.
- [9] P.-O. Schwartz, L. Biniek, E. Zaborova, B. Heinrich, M. Brinkmann, N. Leclerc, S. Méry, J. Am. Chem. Soc. 2014, 136, 5981-5992.
- [10] K. M. Felter, V. M. Caselli, D. D. Günbaş, T, J. Savenije, F. C. Grozema, ACS Appl. Energy Mater. 2019, 2, 8010-8021.
- [11] C. Huang, S. Barlow, S. R. Marder, J. Org. Chem. 2011, 76, 2386-2407.
- [12] R. Schmidt, J. H. Oh, Y.-S. Sun, M. Deppisch, A.-M. Krause, K. Radacki, H. Braunschweig, M. Könemann, P. Erk, Z. Bao, F. Würthner, J. Am. Chem. Soc. 2009, 131, 6215-6228.

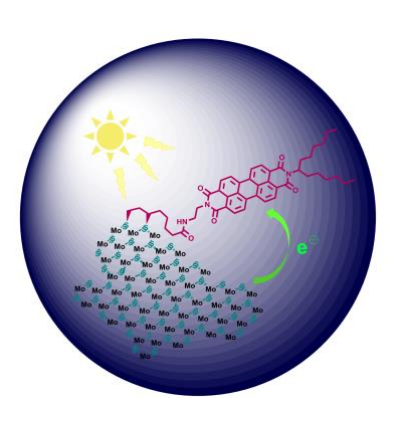
- [13] G. Zhang, J. Zhao, P. C. Y. Chow, K. Jiang, J. Zhang, Z. Zhu, J. Zhang, F. Huang, H. Yan, Chem. Rev. 2018, 118, 3447-3507.
- [14] E. Avellanal-Zaballa, G. Durán-Sampedro, A. Prieto-Castañeda, A. R. Agarrabeitia, I. García-Moreno, I. López-Arbeloa, J. Bañuelos, M. J. Ortiz, Phys. Chem. Chem. Phys. 2017, 19, 13210-13218.
- [15] a) R. Canton-Vitoria, L. Vallan, E. Urriolabeitia, A. M. Benito, W. K. Maser, N. Tagmatarchis, *Chem. Eur. J.* 2018, 24, 10468-10474; b) L. Vallan, R. Canton-Vitoria, H. B. Gobeze, Y. Jang, R. Arenal, A. M. Benito, W. K. Maser, F. D' Souza, N. Tagmatarchis, *J. Am. Chem. Soc.* 2018, 140, 13488-13496.
- [16] a) R. Canton-Vitoria, T. Scharl, A. Stergiou, A. Cadranel, R. Arenal, D. M. Guldi, N. Tagmatarchis, Angew. Chem. Int. Ed. 2020, 59, 3976-3981.
- [17] R. Canton-Vitoria, H. B. Gobeze, V. M. Blas-Ferrando, J. Ortiz, Y. Jang, F. Fernández-Lázaro, Á. Sastre-Santos, Y. Nakanishi, H. Shinohara, F. D'Souza, N. Tagmatarchis, *Angew. Chem. Int. Ed.* 2019, *58*, 5712-5717.
- [18] X. Yu, A. Rahmanudin, X. A. Jeanbourquin, D. Tsokkou, N. Guijarro, N. Banerji, K. Sivula, ACS Energy Lett. 2017, 2, 524-531.
- [19] G. Pagona, C. Bittencourt, R. Arenal, N. Tagmatarchis, *Chem. Commun.* 2015, *51*, 12950-12953.
- [20] S. Bae, N. Sugiyama, T. Matsuo, H. Raebiger, K.-i. Shudo, K. Ohno, Phys. Rev. Appl. 2017, 7, 024001.
- [21] S. Jimenez Sandoval, D. Yang, R. F. Frindt, J. C. Irwin, J. C. Phys. Rev. B 1991, 44, 3955-3962.
- [22] Z. Luo, A. Peng, H. Fu, Y. Ma, J. Yao, B. H. Loo, J. Mater. Chem. 2008, 18, 133-138.
- [23] W. E. Ford, J. Photochem. 1987, 37, 189-204.
- [24] S. Gan, L. Zhong, C. Engelbrekt, J. Zhang, D. Han, J. Ulstrup, Q. Chi, L. Niu, *Nanoscale* 2014, 6, 10516-10523.
- [25] L. Wibmer, S. Lages, T. Unruh, D. M. Guldi, Adv. Mater. 2018, 30, 1706702.
- [26] a) A. Wicklein, A. Lang, M. Muth, M. Thelakkat, J. Am. Chem. Soc. 2009, 131, 14442-14453; b) C. Huang, S. Barlow, S. R. Marder, J. Org. Chem. 2011, 76, 2386-2407.
- [27] L. Marin-Gomis, F. Peralta-Ruiz, M. B. Thomas, F. Fernandez-Lazaro, F. D'Souza, Á. Sastre-Santos, Chem. Eur. J. 2017, 23, 3863-3874.
- [28] W. E. Ford, P. V. Kamat, J. Phys. Chem. 1987, 91, 6373-6380.
- [29] J. J. Snellenburg, S. P. Laptenok, R. Seger, K. M. Mullen, and I. H. M. van Stokkum, J. Stat. Softw. 2012, 49, 1-22.



WILEY-VCH

RESEARCH ARTICLE

Entry for the Table of Contents



A well-known electron acceptor perylenediimide (PDI) is covalently attached to semiconducting MoS_2 exposing the MoS_2 material's electron donating potential in the novel MoS₂-PDI hybrid.

